Equation-of-state, sound speed, and reshock of shock-compressed fluid carbon dioxide

L. E. Crandall,[1,2] J. R. Rygg,[1,2,3] D. K. Spaulding,[4] M. F. Huff,[1,2] M. C. Marshall,[1] D. N. Polsin,[1] R. Jeanloz,[5] T. R. Boehly,[1] M. Zaghoo,[1] B. J. Henderson,[1,2] S. Brygoo,[6] P. M. Celliers,[7] J. H. Eggert,[7] D. E. Fratanduono,[7] A. Lazicki,[7] M. Millot,[7] and G. W. Collins[1,2,3]

[1)] *Laboratory for Laser Energetics, Rochester, New York 14623, USA*

[2)] *Department of Physics, University of Rochester, Rochester, New York 14611, USA*

[3)] *Department of Mechanical Engineering, University of Rochester, Rochester, New York 14611, USA*

[4)] *University of California, Davis, California 95616, USA*

[5)] *University of California, Berkeley, California 94720-5800, USA*

[6)] *CEA, DAM, DIF, F-91297 Arpajon, France*

[7)] *Lawrence Livermore National Laboratory, Livermore, California 94550-9234, USA*

(Dated: 8 December 2020)

Mechanical equation-of-state data of initially liquid and solid CO_2 shock-compressed to terapascal conditions are reported. Diamond-sapphire anvil cells were used to vary the initial density and state of CO_2 samples that were then further compressed with laser-driven shock waves, resulting in a data set from which precise derivative quantities including Grüneisen parameter and sound speed are determined. Reshock states are measured to 800 GPa and map the same pressure-density conditions as the single shock using different thermodynamic paths. The compressibility data reported here do not support current density-functional-theory calculations, but are better represented by tabular equation-of-state models.

I. INTRODUCTION

The covalent double-bonds that bind the atoms in a CO_2 molecule at ambient conditions are among the strongest of chemical bonds, but at pressures reaching tens of GPa, the compression energy ($P\Delta V$) becomes comparable to this bonding energy (hundreds of kJ/mol), and the previously stable molecule exhibits complex chemical behavior.[1,2] Laser-heated diamond-anvil cell experiments have characterized the solid phase diagram of CO_2 up to 120 GPa, which exhibits five molecular crystalline polymorphic phases before transforming into both crystalline and amorphous polymeric phases.[1–7]

The fluid phase diagram of CO_2 has been experimentally explored to 1 TPa[8–13] and is proposed to exhibit similar chemical complexity to the solid phase diagram.[14] When shock compressed, molecular liquid CO_2 (Fluid-I) is stable up to 40 GPa,[8,10] above which it transforms into an insulating 3- and 4-coordinated polymeric fluid (Fluid-II).[11,14] Above 100 GPa, CO_2 transitions into the Fluid-III phase and begins to ionize.[13] The present work is a study of the Fluid-III phase of CO_2.

The pressure, density, temperature, and reflectivity of shocked CO_2 have been measured to 1 TPa and 93,000 K in Ref. 13. Experimental evidence indicates that CO_2 at the highest pressures and temperatures studied is in a complex bonded state as opposed to the previously predicted[12] fully atomic C, O fluid. This work reports further details of the study presented in Ref. 13, and additionally reports the experimentally determined Grüneisen parameter and isentropic sound speed of shocked CO_2, and the mechanical behavior of CO_2 under reshock.

II. EXPERIMENTAL METHOD

These experiments took place on the OMEGA Laser System at the Laboratory for Laser Energetics in Rochester, NY.[15] The laser-shocked diamond-sapphire anvil cell[16–20] containing the precompressed CO_2 sample is depicted in Fig. 1. The CO_2 samples were cryogenically loaded into cells comprising 350-μm-thick diamond and 5000-μm-thick sapphire anvils. The CO_2 was contained between the anvils in a stainless-steel gasket. The gasket was initially 250-μm thick; after compression, the gasket thickness was reduced to approximately 150 μm. The anvils were mounted in tungsten carbide (WC) seats; the diamond side seat had a 900-μm lateral window, and the sapphire side seat had an 800-μm window. The diamond was coated with 3 μm of gold and a 15-μm plastic ablator; the gold served to absorb x-rays produced at the ablation front and prevent photoionization of the sample. Two 25-μm-thick α-quartz pieces, referred to as the pusher and the window, were located in the sample chamber with the CO_2. The quartz pusher served as an impedance matching,[21] reflectivity, and temperature standard[22–25] for singly shocked CO_2. The quartz rear window allowed for the determination of a reshock state in the CO_2.

The loaded cell was mechanically compressed to pressures of 0.36 to 1.16 GPa at ambient temperature. These pressures correspond to densities in the CO_2 ranging from 1.35 g/cm^3 (Ref. 26) to 1.74 g/cm^3 (Refs. 5 and 7), and densities in the quartz ranging from 2.68 g/cm^3 and 2.73 g/cm^3 (Ref. 24). Above 0.5 GPa, CO_2 crystallizes into solid phase-I.[6] The formation of crystals in the CO_2 was observed in cells with the highest precompression. The precompression pressures were measured using calibrated fluorescence spectroscopy of ruby beads within the cell[27] and the density of the CO_2 was then determined from a 295K isotherm.[5–7,26]

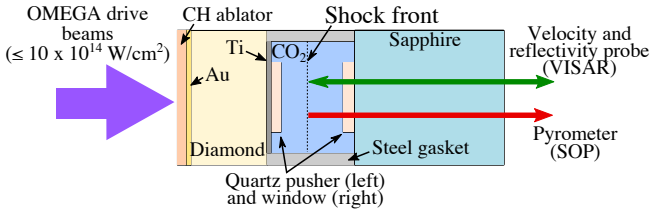

FIG. 1. CO_2 was precompressed in diamond-sapphire anvil cells before being shock compressed to TPa conditions with the OMEGA laser. The primary diagnostics were VISAR (velocity interferometer system for any reflector) and SOP (streaked optical pyrometry). The components of the diamond-sapphire anvil cell depicted in the cartoon are described in the text.

The OMEGA laser irradiated the plastic ablator with intensities between 1.2 x 10^{14} W/cm^2 and 10.0 x 10^{14} W/cm^2; these experiments used 12 beams with up to 480 J per beam (5760 J total) in an 865-μm focal spot and a 1-ns pulse duration. The laser ablation of the CH layer drove shock waves through the diamond anvil and quartz pusher into the liquid or solid CO_2 sample. The pressures in these experiments were sufficiently high to ionize the CO_2 and produce an optically reflective shock front.

The velocity of the reflecting shock front was measured with a dual-channel line-imaging velocity interferomer system for any reflector (VISAR).[28] The apparent velocity from VISAR is corrected for the precompressed refractive index of quartz[24] and CO_2.[6,7] The dual-interferometer system allows one to resolve 2π fringe ambiguities and determine a unique velocity solution. Integrating the velocity as a function of time must yield the thickness of the quartz and CO_2 sample chamber; this serves as another check on the velocity solution.

Impedance matching[21] was performed at the quartz pusher/CO_2 interface using the Rankine–Hugoniot conditions for conservation of mass, momentum, and energy to calculate the particle velocity, pressure, density, and internal energy in the shocked CO_2. A Mie–Grüneisen linear release[22,24] was used to model the release of the higher-impedance quartz into the lower-impedance CO_2. Additionally, the intensity of the VISAR signal is used to determine the reflectivity of the shocked CO_2 at 532 nm by referencing to the known quartz reflectivity as a function of shock velocity.[24,25]

Simultaneously with the VISAR, the self-emission (590 to 850 nm) from the shock front was measured using streaked optical pyrometry (SOP),[29,30] from which a brightness temperature was determined. Brightness temperature is inferred from the measured emission with the assumption that the shock front emits as a grey body with reflectivity as measured with VISAR. While particle velocity, density, and pressure are determined from impedance matching only at the instant the shock wave is transmitted from the quartz pusher into the CO_2, shock velocity, temperature, and reflectivity are tracked continuously through the shock transit of the entire experiment.

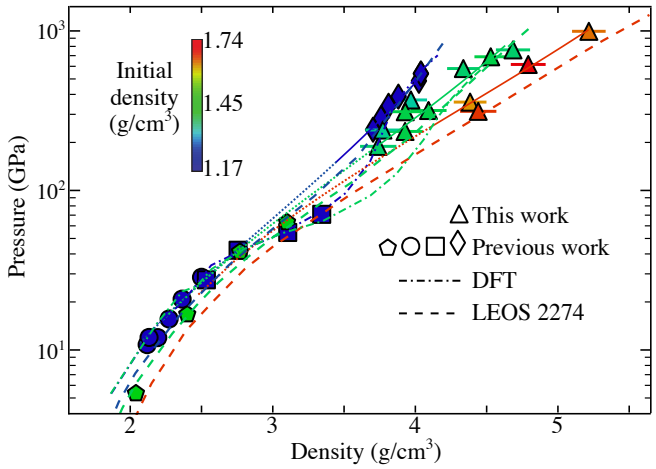

FIG. 2. Log pressure versus density for shocked CO_2. Triangles are these OMEGA data, diamonds are Sandia Z data,[12] and pentagons[8], circles[10], and squares[11] are gas-gun data. Also plotted are LEOS (dashed) and density functional theory (DFT) (dashed–dotted) calculations. Solid lines are the Eq. (1) fit to the OMEGA and Z data; dotted lines extrapolate this fit to lower pressure. Initial density of all data points and curves is given by the color bar.

$c_0(\frac{km}{s})$	s	$a(\frac{km}{s}\frac{cm^3}{g})$
–1.88	1.29	3.36
$\sigma^2_{c_0}$	σ^2_s	σ^2_a
7.06e–02	7.85e–05	3.30e–02
$\sigma_{c_0}\sigma_s$	$\sigma_{c_0}\sigma_a$	$\sigma_s\sigma_a$
–1.30e–03	–4.21e–02	1.32e–04

TABLE I. Parameters and covariance matrix elements for Eq. (1).[13]

III. SINGLE-SHOCK COMPRESSIBILITY RESULTS AND DISCUSSION

The pressure and density results from these experiments are plotted in Fig. 2 (triangles), along with previous CO_2 single-shock data.[8–11] We performed a linear fit to the shock velocity (U_S) versus particle velocity (U_P) data between 189 and 995 GPa (this work and Ref. 12) with a linear term to account for variation in initial density ρ_0:

$$U_S(U_P,\rho_0) = c_0 + sU_P + a\rho_0. \quad (1)$$

The data all lie within 2-σ of the fit. Other fits, including quadratic, cubic, and exponential, were performed, but statistical analysis showed that the data did not justify a fit more complex than linear. Parameters and covariance matrix elements for Eq. (1) are given in Table I.

This fit was converted to pressure versus density using the Rankine–Hugoniot conservation relations and plotted in Fig. 2 with solid lines, and extrapolated to lower pressure with dotted lines. Quantum mechanical calculations [density function theory, (DFT),[31] dashed–dotted lines], benchmarked by Ref. 11 (squares), predict significant curvature between 50 and 500 GPa. Our measurements from initially 1.4 g/cm^3

(green) do not support such curvature and are in better agreement with LEOS models.[32] LEOS table 2274, constructed using the quotidian equation-of-state methodology, expresses the Helmholtz free energy as a function of volume and temperature, and includes a dissociation term and a non-dissociation term in the ion free energy.[32] These terms are coupled by the molar mass. It is significant that the LEOS table represents the mechanical behavior of the data in the present work, but does not represent the increase in compressibility seen by Ref. 11.

There exists a clear anomaly in the low-pressure gas-gun data from Ref. 11 (blue squares) and Ref. 8 (green pentagons) seen in Fig. 2. For a given shock pressure, it is expected that CO_2 of a higher initial density will have a higher final density due to reduced heating. The low-pressure data demonstrate this behavior until 42 GPa; above this pressure, the data from Ref. 11 (blue squares) show a higher final density for a given shocked pressure than the data from Ref. 8, despite having a lower initial density. The high-pressure data (this work and Ref. 12, 189 to 995 GPa) demonstrate the expected behavior. The anomaly in the gas-gun data has led to disagreement in the modeling of CO_2, and the present measurements support LEOS[32] over current DFT[31] calculations in the high-pressure fluid regime.

IV. GRÜNEISEN PARAMETER AND SOUND SPEED

Variation in initial density was leveraged to measure multiple Hugoniot curves, from which derivative quantities were probed using a difference method.[25] The Grüneisen parameter $\gamma = V\frac{\partial P}{\partial E}|_V$ was determined from the mechanical equation-of-state given by Eq. (1) and a difference method between initially 1.17 and 1.4 g/cm^3; 1.17 and 1.7 g/cm^3; and 1.4 and 1.7 g/cm^3 Hugoniots. The Grüneisen parameter shows little dependence on initial density; all three difference methods yield the same result within 10%. The averaged result is plotted in Fig. 3(a) with a 1-σ confidence interval based on the uncertainty in the U_S–U_P fit. Additionally plotted are predictions of γ from tabular equations-of-state SESAME 5212 and LEOS 2274.[32] Theoretical γ is systematically higher than the experimental result, but all curves tend to the ideal gas limit of $2/3$.

The isentropic sound speed can be directly calculated from the measured Hugoniot and Grüneisen paramater γ with:[33]

$$C_s^2 = V^2 \frac{\frac{\gamma}{2V} - P_H - \frac{dP}{dV}|_H (V_0 - V)}{\frac{dP}{dV}|_H}. \quad (2)$$

C_s was calculated from Eqs. (1) and (2) for three different initial densities: 1.17 g/cm^3, 1.4 g/cm^3, and 1.7 g/cm^3. The sound speed on the Hugoniot from each initial density differed by less than 3%, showing even less dependence on initial density than the Grüneisen parameter. The averaged result is plotted in Fig. 3(b) with a 1-σ confidence interval propogated from the uncertainty in the parameters in Eq. (1) and the uncertainty in γ with a 10,000 trial Monte Carlo method.

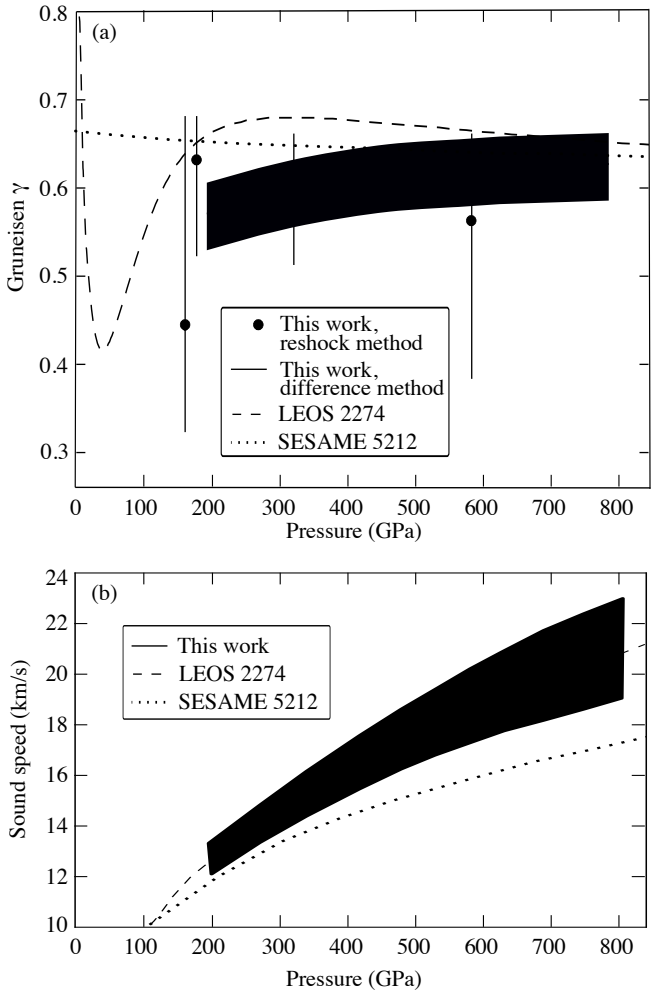

FIG. 3. (a) The Grüneisen parameter γ in shocked CO_2. This work (solid line) calculated γ from Eq. (1) using a difference method between Hugoniots of different initial densities. Theoretical curves LEOS[32] (dashed line) and SESAME (dotted line) reasonably represent this experimental work. Also plotted (points) is γ as determined from the reshock model in Eq. (4). (b) Sound speed of shocked CO_2. This work (solid line) calculates sound speed from Eq. (2) and γ. LEOS[32] (dashed line) shows excellent agreement with these results, while SESAME (dotted line) underpredicts the sound speed.

SESAME 5212, a single-phase equation-of-state, underpredicts the sound speed of shocked CO_2, but LEOS 2274[32] shows excellent agreement with our experimental data. This is expected given the good agreement between LEOS 2274[32] and our Hugoniot data.

V. RESHOCK RESULTS AND DISCUSSION

When the shock wave traverses the CO_2 sample and enters the higher-impedance quartz rear window, a second shock (reshock) is launched back into the CO_2 sample. Impedance matching[21] is performed at the CO_2/window interface to determine the pressure, density, and internal energy of this reshock in CO_2. The shock velocity of the CO_2 (U_{S,CO_2}) and

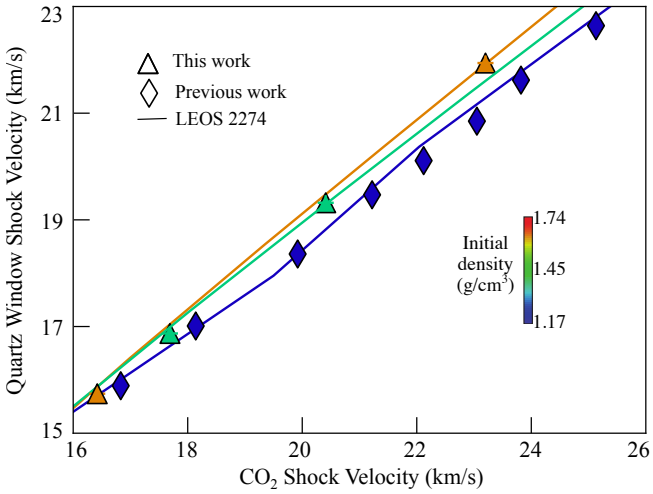

FIG. 4. Shock velocity in the quartz window versus shock velocity in the CO_2 sample on either side of their interface. A reshock is launched back into the CO_2 sample when the shock traverses into the higher impedance quartz window. Triangles are these OMEGA data and diamonds are Sandia Z data.[12] Solid lines are LEOS[32] curves based on the modeled reshock intersecting with the experimental quartz Hugoniot.[23,24] Uncertainty in the solid curves based on uncertainty in the quartz Hugoniot is less than 0.5%. Initial density of all points and curves is given by the color bar.

the quartz window ($U_{S,Q}$) are measured on either of the interface with VISAR. From the known quartz Hugoniot[23,24] and Eq. (1) for an initial density of ρ_{0,CO_2}, the pressure, density, and particle velocity on either side of the interface for both CO_2 (P_{CO_2}, ρ_{CO_2}, U_{P,CO_2}) and quartz (P_Q, ρ_Q, $U_{P,Q}$) are also known. By impedance matching, the pressure of the reshocked CO_2 (P_R) must be equal to P_Q. By the Rankine-Hugoniot conservation relations, the density of the reshocked CO_2 (ρ_R) is given by:

$$\rho_R = \frac{\rho_{CO_2}(P_Q - P_{CO_2})}{P_Q - P_{CO_2} - \rho_{CO_2}(U_{P,Q} - U_{P,CO_2})^2}. \quad (3)$$

The present work measured four reshock states in CO_2, which are summarized in Table II. The reshock results from this work and from Ref. 12 are summarized in Figs. 4 and 5. The experimental observables U_{S,CO_2} and $U_{S,Q}$ are plotted in Fig. 4 along with LEOS curves[32] based on intersection of the modeled reshock with the experimental quartz Hugoniot.[23,24] This work shows strong agreement with LEOS, as does most of the data from Ref. 12.

Figure 5(a) represents the reshock data in the pressure-density plane. The pressure along a reshock curve is related to the pressure on the Hugoniot at the same specific volume V (inverse of density, ρ) by assuming a constant γ equation of state:[34]

$$P_R = \frac{\frac{V}{\gamma}P_H + \frac{1}{2}(P_1 - P_H)(V_0 - V)}{\frac{V}{\gamma} - \frac{1}{2}(V_1 - V)}. \quad (4)$$

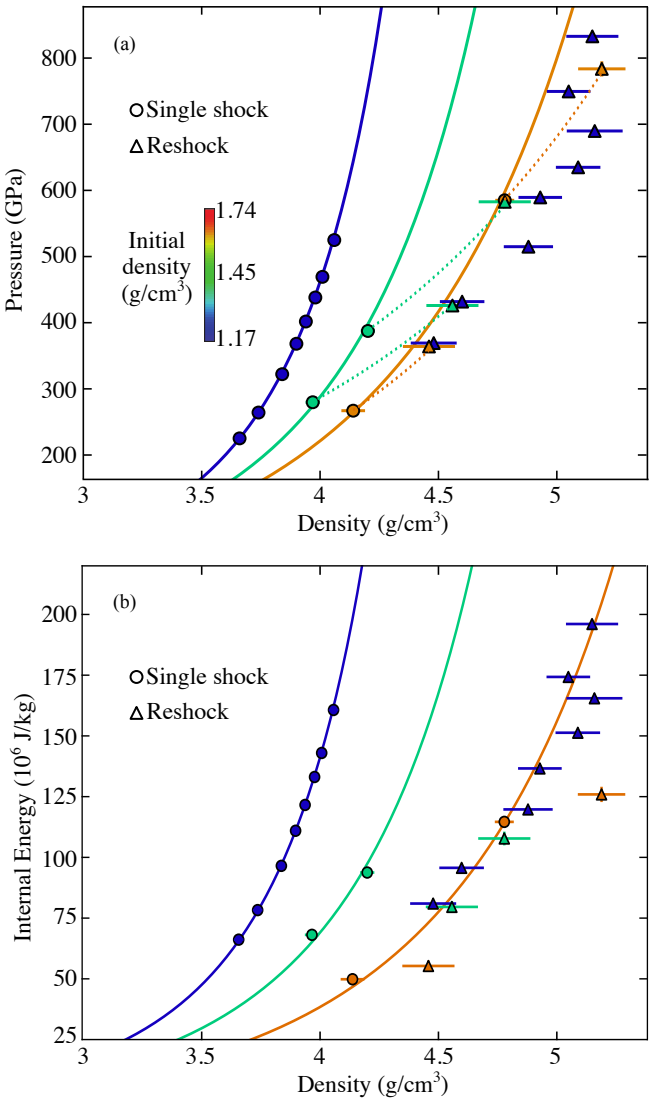

FIG. 5. [(a), (b)] Reshock results from this work (green and orange data points) and Ref. 12 (blue data points). Circles are the single-shocked state in CO_2 immediately before shock transmission into the quartz window; triangles are the reshocked state in CO_2. Solid lines are the CO_2 single-shock Hugoniot given by Eq. (1) for ρ_0 = 1.167 (blue), 1.375 (green), and 1.655 (orange) g/cm^3; dotted lines are the reshock curves of CO_2 given by Eq. (4). Color represents initial density as given by the color bar. Note that the green and orange single-shock CO_2 points have varying initial densities given by Table II, and therefore do not sit exactly on the plotted Hugoniots. Error bars in pressure and energy are smaller than the data points.

where V_0 is the initial specific volume ($1/\rho_0$); P_R is the pressure on the reshock curve at volume V from initial state P_1,V_1 on the principle Hugoniot; P_H is the pressure on the principle Hugoniot at volume V; and γ is the Grüneisen parameter. Because the single-shock and reshocked state of CO_2 were determined with impedance matching, Eq. (4) serves as an independent way to determine γ, plotted in Fig. 3(a) (points). The uncertainty in γ represents how much γ can vary and still yield the measured reshocked state in the CO_2 within

Shot	$U_{S,Q}$ (km/s)	U_{S,CO_2} (km/s)	ρ_{0,CO_2} (g/cm^3)	P_1 (GPa)	ρ_1 (g/cm^3)	P_R (GPa)	ρ_R (g/cm^3)
58917	15.74 (0.14)	16.42 (0.14)	1.64 (0.01)	267 (6)	4.14 (0.05)	364 (7)	4.46 (0.11)
57510	16.87 (0.14)	17.69 (0.14)	1.36 (0.01)	280 (6)	3.97 (0.03)	426 (8)	4.56 (0.11)
58920	19.32 (0.14)	20.41 (0.14)	1.39 (0.01)	388 (6)	4.20 (0.03)	583 (10)	4.78 (0.11)
58922	21.94 (0.14)	23.20 (0.14)	1.67 (0.01)	585 (9)	4.78 (0.05)	784 (12)	5.19 (0.11)

TABLE II. Results for reshocked CO_2. Experimental observables are the shock velocity in the CO_2 and quartz window on either side of their interface (U_{S,CO_2} and $U_{S,Q}$). The initial density in the CO_2 is given by ρ_{0,CO_2}. The pressure and density in the CO_2 immediately before the shock enters the quartz window are given by P_1 and ρ_1. The pressure and density in the reshocked CO_2 are given by P_R and ρ_R.

the error bar. The results are consistent with those obtained from a difference method applied to the CO_2 single-shock equation-of-state [Fig. 3(a) solid line], but P_R in Eq. (4) does not provide strong constraints on γ given present uncertainties in the measured density of reshocked CO_2. Reshock curves for the best value of γ are plotted in Fig. 5 (dotted).

There are three pairs of data points in Fig. 5(a) that reach the same pressure-density state following different thermodynamic paths. As shown in Fig. 5(b), when plotted as internal energy versus density, those points no longer overlap, implying that the states are at different temperatures. Internal energy was determined from the Rankine–Hugoniot condition for conservation of energy. To account for the different initial energy arising from different initial conditions, the initial energy for initially liquid points [blue and green in Fig. 5(b)] was taken from Ref. 35 [–421 J/g for initially 220 K and 1.167 g/cm^3 (blue) and –393 J/g for initially 295 K and 1.39 g/cm^3 (green)]. The initial energy in the initially solid (orange) points was then found by shifting from the initially liquid (green) points on a 295 K isotherm by integrating the pressure–volume curves from Refs. 5,6 and adding the latent heat of fusion from Ref. 36, to yield –552 J/g for initially 295 K and 1.67 g/cm^3. In all cases, the initial internal energy of the CO_2 was approximately 50% of the error bar of the final shocked internal energy.

Because Eq. (4) relates pressure on the Hugoniot to pressure on the reshock curve at the same volume, the model fails beyond maximum compression of the principle Hugoniot. For this reason, Eq. (4) cannot be used to determine γ from the reshock data in Ref. 12. There is reshock data reported on CO_2 in Ref. 10 from aluminum and stainless-steel anvils, but the data have significant scatter and no reported uncertainty, so was not included here.

VI. CONCLUSIONS

To summarize, this work provides additional details on recently published[13] equation-of-state measurements of shock compressed CO_2 to 1 TPa and 93,000 K from varying initial densities, and presents new information on the Grüneisen parameter, sound speed, and reshock behavior of high-pressure shocked CO_2. We find that the compressibility, Grüneisen parameter, and sound speed of shocked CO_2 are well represented by LEOS;[32] this work does not support the extreme curvature in compressibility modeled by DFT.[31] Notably, lower-pressure gas-gun data support DFT over LEOS. We discuss an anomaly in the lower-pressure CO_2 data, which has led to disagreement among models. This complexity in the compressibility behavior of shocked CO_2 warrants further study, since there is currently a gap between 71 and 189 GPa where no data exist to constrain theory. We report four reshock states of CO_2, and discuss the effect of the Grüneisen parameter on the reshock curve. This work provides significant new benchmarks for theoretical calculations of fluids in the warm-dense-mater regime.

VII. ACKNOWLEDGMENTS

This material is based upon work supported by the Department of Energy National Nuclear Security Administration under Award Number DE-NA0003856, the University of Rochester, the New York State Energy Research and Development Authority, NNSA support to the University of California, Berkeley, and NSF 19-528 Physics Frontier Centers, Award Number 2020249, Center for Matter at Atomic Pressures. This work was performed under the auspices of the U.S. Department of Energy by Lawrence Livermore National Laboratory under Contract DE-AC52-07NA27344 and was supported by the LLNL-LDRD Program under Project No. 12-SI-007.

This report was prepared as an account of work sponsored by an agency of the U.S. Government. Neither the U.S. Government nor any agency thereof, nor any of their employees, makes any warranty, express or implied, or assumes any legal liability or responsibility for the accuracy, completeness, or usefulness of any information, apparatus, product, or process disclosed, or represents that its use would not infringe privately owned rights. Reference herein to any specific commercial product, process, or service by trade name, trademark, manufacturer, or otherwise does not necessarily constitute or imply its endorsement, recommendation, or favoring by the U.S. Government or any agency thereof. The views and opinions of authors expressed herein do not necessarily state or reflect those of the U.S. Government or any agency thereof.

VIII. DATA AVAILABILITY

The data that support the findings of this study are available from the corresponding author upon reasonable request.

[1] F. Datchi and G. Weck, Z. Kristallogr. **229**, 135 (2014).
[2] C.-S. Yoo, Phys. Chem. Chem. Phys. **15**, 7949 (2013).
[3] K. D. Litasov, A. F. Goncharov, and R. J. Hemley, Earth Planet. Sci. Lett. **309**, 318 (2011).

[4]K. F. Dziubek, M. Ende, D. Scelta, R. Bini, M. Mezouar, G. Garbarino, and R. Miletich, Nat. Commun. **9**, 3148 (2018).
[5]V. M. Giordano, F. Datchi, F. A. Gorelli, and R. Bini, J. Chem. Phys. **133**, 144501 (2010).
[6]V. M. Giordano, F. Datchi, and A. Dewaele, J. Chem. Phys. **125**, 054504 (2006).
[7]H. Shimizu, T. Kitagawa, and S. Sasaki, Phys. Rev. B **47**, 11567 (1993).
[8]V. N. Zubarev and G. S. Telegin, Sov. Phys.-Dokl. **7**, 34 (1962).
[9]Zubarev and Telegin[8] report two different initial densities for their solid CO_2: 1.45 and 1.54 g/cm^3. Cited in Schott[10] are "verbal inquires and replies conveyed through C. L. Mader and A . N. Dremin, *ca.* 1983" that confirm that 1.54 g/cm^3 is a misprint, and the initial density of the data published by Zubarev and Telegin is 1.45 g/cm^3.
[10]G. L. Schott, High Press. Res. **6**, 187 (1991).
[11]W. J. Nellis, A. C. Mitchell, F. H. Ree, M. Ross, N. C. Holmes, R. J. Trainor, and D. J. Erskine, J. Chem. Phys. **95**, 5268 (1991).
[12]S. Root, K. R. Cochrane, J. H. Carpenter, and T. R. Mattsson, Phys. Rev. B **87**, 224102 (2013).
[13]L. E. Crandall, J. R. Rygg, D. K. Spaulding, T. R. Boehly, S. Brygoo, P. M. Celliers, J. H. Eggert, D. E. Fratanduono, B. J. Henderson, M. F. Huff, R. Jeanloz, A. Lazicki, M. C. Marshall, D. N. Polsin, M. Zaghoo, M. Millot, and G. W. Collins, Phys. Rev. Lett. **125**, 165701 (2020).
[14]B. Boates, A. M. Teweldeberhan, and S. A. Bonev, Proc. Natl. Acad. Sci. **109**, 14808 (2012).
[15]T. R. Boehly, D. L. Brown, R. S. Craxton, R. L. Keck, J. P. Knauer, J. H. Kelly, T. J. Kessler, S. A. Kumpan, S. J. Loucks, S. A. Letzring, F. J. Marshall, R. L. McCrory, S. F. B. Morse, W. Seka, J. M. Soures, and C. P. Verdon, Opt. Commun. **133**, 495 (1997).
[16]P. Loubeyre, P. M. Celliers, D. G. Hicks, E. Henry, A. Dewaele, J. Pasley, J. Eggert, M. Koenig, F. Occelli, K. M. Lee, R. Jeanloz, D. Neely, A. Benuzzi-Mounaix, D. Bradley, M. Bastea, S. Moon, and G. W. Collins, High Pres. Res. **24**, 25 (2003).
[17]J. Eggert, S. Brygoo, P. Loubeyre, R. S. McWilliams, P. M. Celliers, D. G. Hicks, T. R. Boehly, R. Jeanloz, and G. W. Collins, Phys. Rev. Lett. **100**, 124503 (2008).
[18]P. M. Celliers, P. Loubeyre, J. H. Eggert, S. Brygoo, R. S. McWilliams, D. G. Hicks, T. R. Boehly, R. Jeanloz, and G. W. Collins, Phys. Rev. Lett. **104**, 184503 (2010).
[19]P. Loubeyre, S. Brygoo, J. Eggert, P. M. Celliers, D. K. Spaulding, J. R. Rygg, T. R. Boehly, G. W. Collins, and R. Jeanloz, Phys. Rev. B **86**, 144115 (2012).
[20]M. Millot, S. Hamel, J. R. Rygg, P. M. Celliers, G. W. Collins, F. Coppari, D. E. Fratanduono, R. Jeanloz, D. C. Swift, and J. H. Eggert, Nat. Phys. **14**, 297 (2018).
[21]Ya. B. Zel'dovich and Yu. P. Raĭzer, in *Physics of Shock Waves and High-Temperature Hydrodynamic Phenomena*, edited by W. D. Hayes and R. F. Probstein (Dover Publications, Mineola, NY, 2002).
[22]M. D. Knudson and M. P. Desjarlais, Phys. Rev. B **88**, 184107 (2013).
[23]M. P. Desjarlais, M. D. Knudson, and K. R. Cochrane, J. Appl. Phys. **122**, 035903 (2017).
[24]S. Brygoo, M. Millot, P. Loubeyre, A. E. Lazicki, S. Hamel, T. Qi, P. M. Celliers, F. Coppari, J. H. Eggert, D. E. Fratanduono, D. G. Hicks, J. R. Rygg, R. F. Smith, D. C. Swift, G. W. Collins, and R. Jeanloz, J. Appl. Phys. **118**, 195901 (2015).
[25]D. G. Hicks, T. R. Boehly, J. H. Eggert, J. E. Miller, P. M. Celliers, and G. W. Collins, Phys. Rev. Lett. **97**, 025502 (2006).
[26]S. M. Sterner and K. S. Pitzer, Contrib. Mineral. Petr. **117**, 362 (1994).
[27]G. J. Piermarini, S. Block, J. D. Barnett, and R. A. Forman, J. Appl. Phys. **46**, 2774 (1975).
[28]P. M. Celliers, D. K. Bradley, G. W. Collins, D. G. Hicks, T. R. Boehly, and W. J. Armstrong, Rev. Sci. Instrum. **75**, 4916 (2004).
[29]J. E. Miller, T. R. Boehly, A. Melchior, D. D. Meyerhofer, P. M. Celliers, J. H. Eggert, D. G. Hicks, C. M. Sorce, J. A. Oertel, and P. M. Emmel, Rev. Sci. Instrum. **78**, 034903 (2007).
[30]M. C. Gregor, R. Boni, J. Kendrick, C. A. McCoy, D. N. Polsin, T. R. Boehly, P. M. Celliers, D. E. Fratanduono, J. H. Eggert, and M. Millot, Rev. Sci. Instrum. **87**, 114903 (2016).
[31]B. Boates, S. Hamel, E. Schwegler, and S. A. Bonev, J. Chem. Phys. **134**, 064504 (2011).
[32]C. J. Wu, D. A. Young, P. A. Sterne, and P. C. Myint, J. Chem. Phys. **151**, 224505 (2019).
[33]C. A. McCoy, M. C. Marshall, D. N. Polsin, D. E. Fratanduono, P. M. Celliers, D. D. Meyerhofer, and T. R. Boehly, Phys. Rev. B **100**, 014106 (2019).
[34]R. G. McQueen, S. P. Marsh, J. W. Taylor, J. N. Fritz, and W. J. Carter, in *High-Velocity Impact Phenomena*, edited by R. Kinslow (Academic Press, New York, 1970).
[35]R. Span and W. Wagner, J. Phys. Chem. Ref. Data **25**, 1509 (1996).
[36]J. Ancsin, Metrologia **29**, 71 (1992).